PIER C

An Improved Equivalent-Input-Disturbance Method Based on Enhanced Estimators for Wideband Disturbance Suppression in PMSM

Jiacheng Tong, Kaihui Zhao*, Yunzhen Chen, Jinnan Cao, Youzhuo Duan, and Jie Xiong

School of Transportation and Electrical Engineering, Hunan University of Technology, China

ABSTRACT: This paper presents an improved equivalent-input-disturbance (IEID) method based on enhanced estimators. This method addresses the degradation performance in a permanent magnet synchronous motor (PMSM) drive system caused by multi-source disturbances in different frequency bands. First, a PMSM model is established that considers these disturbances and categorizes them as control inputs for both current and speed loops. Next, the estimated compensation structures of the dual-loop equivalent-input-disturbance (EID) are designed. To address the differing sensitivities of the dual-loop anti-disturbance frequency bands, enhanced estimators are designed to expand their respective bandwidths. This reduces the sensitivity of the system to uncertainty, and parameter-adjusting conditions are derived to ensure stability. Finally, the simulation results demonstrate that, when PMSM operates under the nominal condition, the IEID method suppresses steady-state speed fluctuation by approximately 63% compared to the method without EID compensation, by approximately 35% compared to the conventional EID method, and by approximately 25% compared to improved sliding mode observer-based EID (ISMO-EID) method; when PMSM parameters are perturbed, the suppression rates can further reach to 65%, 44%, and 32%, respectively. The findings indicate that the proposed method exhibits superior steady-state tracking accuracy and disturbance suppression performance, while also exhibiting enhanced robustness in transient scenarios.

1. INTRODUCTION

To meet the demands of the modern industry for energy-efficient motors, PMSM has become widely used in many fields, including industrial servo, household appliances, aerospace, and new energy applications, owing to its simple structure, high efficiency, high power density, and excellent control performance [1].

However, in high-performance application scenarios, PMSM drive system is affected by both nonlinear internal disturbances, such as magnetic flux harmonics [2], cogging effects [3], sensor and inverter nonlinearity [4, 5], motor mechanical properties [6], and model uncertainties caused by parameter perturbation. In such circumstances, the conventional control method significantly impairs steady-state and transient performance of the motor when facing complex external load changes. To ensure the stability and efficient operation of a PMSM drive system, a disturbance suppression control method must be developed.

Advanced control technologies, such as adaptive robust control [7] and sliding mode control [8], have been used in the field of motor control to improve its anti-disturbance ability and robustness. However, because of the complexity of disturbances, these passive anti-disturbance methods require a large controller gain, which inevitably leads to other performance losses.

To solve this problem, several active disturbance suppression mechanisms exist, including disturbance observer-based con-

trol [9], active disturbance rejection control (ADRC) [10], and the equivalent-input-disturbance (EID) methods [11]. Among these methods, the EID method is least dependent on the nominal model. It does not require one to consider external or internal disturbances. Structurally, only a state observer and a filter are required to reconstruct the virtual disturbance signal equivalent to the external disturbance using the system state. This makes the EID method relatively simple to implement [12].

In a PMSM drive system, considering multi-source disturbances, the use of multiple EID frameworks can achieve disturbance suppression. However, owing to the varying frequencies of multi-source disturbances, applying a low-pass filter to each EID framework is undoubtedly ineffective. A detailed frequency analysis was conducted on a multi-source disturbance model for a PMSM [1]. The analysis concluded that the disturbances primarily consisted of the motor's fundamental frequency and its harmonics, the motor's rotational frequency and its harmonics, and some aperiodic components. Therefore, our research focuses on improving the conventional EID method to expand its disturbance-suppression bandwidth.

Modifying and optimizing the filter configuration is a simple and feasible way to enhance the EID performance. An improved estimator was designed to cancel out the effects of disturbances and nonlinearities in the low-frequency domain, thereby making the system design more flexible [13]. Owing to the low-pass property of the closed-loop system linear part, high-frequency effects are filtered out. A new filter was designed for the improved EID estimator to eliminate the band-

width constraint, ensuring that the sensitivity of the system to disturbances decreases freely at low frequencies [14].

This paper presents an improved equivalent-input-disturbance (IEID) method based on enhanced estimators that improves the disturbance suppression across different frequency bands for a PMSM drive system with multi-source disturbances.

The main contributions of this study are as follows.

(i) The IEID estimation compensation structures for the current and speed loops are designed. Furthermore, the IEID anti-disturbance mechanism of the current and speed loops is analyzed.

(ii) Different enhanced estimators for the current and speed loops are designed to reduce the relative order of the external disturbance sensitivity function to 1. This improves the ability of the EID to suppress the disturbances across different frequency bands and reduces the system's sensitivity to uncertainties.

(iii) The impact of system uncertainties on stability is analyzed, and the parameter-adjusting criteria in conjunction with a proportional-integral (PI) controller are derived to ensure system stability.

The remainder of this paper is organized as follows. Section 2 establishes the PMSM model that considers multi-source disturbances. Section 3 describes the implementation of the EID method and analyzes its anti-disturbance mechanisms. Section 4 presents the IEID method and analyzes the stability of the system. Section 5 presents the simulation results. Finally, Section 6 concludes the study.

2. MATHEMATICAL MODEL OF PMSM WITH MULTI-SOURCE DISTURBANCES

2.1. Ideal Model of PMSM

Ignoring hysteresis, eddy current losses, and nonlinear factors, such as system disturbances, the mathematical model of an ideal PMSM in a *d-q* reference frame is

$$
\begin{cases}
\dfrac{di_d}{dt} = -\dfrac{R_{so}}{L_{do}}i_d + \dfrac{1}{L_{do}}u_d + \dfrac{L_{qo}}{L_{do}}n_p\omega_m i_q \\[2mm]
\dfrac{di_q}{dt} = -\dfrac{R_{so}}{L_{qo}}i_q + \dfrac{1}{L_{qo}}u_q - \dfrac{n_p\omega_m}{L_{qo}}\left[L_{do}i_d + \psi_{ro}\right] \\[2mm]
\dfrac{d\omega_m}{dt} = \dfrac{1}{J_o}\left[T_e - T_L - B_m\omega_m\right] \\[2mm]
T_e = \dfrac{3n_p}{2}\left[\psi_{ro} + (L_{do} - L_{qo})\,i_d\right]i_q
\end{cases} \tag{1}
$$

where

i_d, i_q: *d*- and *q*-axis stator currents (A);

u_d, u_q: *d*- and *q*-axis stator voltages (V);

L_{do}, L_{qo}: *d*- and *q*-axis nominal inductances (H);

R_{so}: nominal stator resistance (Ω);

ψ_{ro}: nominal PM flux (Wb);

J_o: nominal rotational inertia (kg · m^2);

n_p: number of pole pairs (pairs);

B_m: viscous friction coefficient (Nm · s/rad);

ω_m: mechanical angular velocity (rad/s);

T_e: electromagnetic torque (N · m);

T_L: load torque (N · m).

2.2. Model of PMSM with Multi-Source Disturbances

Multi-source disturbances can be divided into two categories based on their source. The first includes external disturbances, such as magnetic flux harmonics [2], cogging effect [3], current sensor measurement error [4], inverter dead-time effect [5], motor mechanical properties [6], and load variations. These disturbances can be regarded as being imposed on the control input channel. The second category includes parameter perturbation and other system uncertainties.

When using vector control with $i_d = 0$, the PMSM model with multi-source disturbances is

$$
\begin{cases}
\dot{\mathbf{x}} = \mathbf{A}\mathbf{x} + \mathbf{B}\mathbf{u} + \mathbf{d}^{total} \\
\mathbf{y} = \mathbf{C}\mathbf{x}
\end{cases} \tag{2}
$$

where $\mathbf{x} = [i_d\ i_q\ \omega_m]^{\mathrm{T}}$ is a vector of the system state; $\mathbf{u} = [u_d^*\ u_q^*\ i_q^*]^{\mathrm{T}}$ is a vector of the control input; $\mathbf{A} = \mathbf{A}_o + \Delta\mathbf{A}(t)$ and $\mathbf{B} = \mathbf{B}_o + \Delta\mathbf{B}(t)$ are the input matrices; $\mathbf{A}_o = \mathrm{diag}(a_{do}, a_{qo}, 0)$, $a_{do} = -R_{so}/L_{do}$, $a_{qo} = -R_{so}/L_{qo}$; $\mathbf{B}_o = \mathrm{diag}(b_{do}, b_{qo}, b_{\omega o})$, $b_{do} = 1/L_{do}$, $b_{qo} = 1/L_{qo}$, $b_{\omega o} = 3n_p\psi_{ro}/2J_o$; $\mathbf{C} = \mathrm{diag}(1, 1, 1)$; $\Delta\mathbf{A}(t)$ and $\Delta\mathbf{B}(t)$ represent the time-varying perturbation of the motor parameter.

The defined $\mathbf{d}^{total} = [d_d^{total}\ d_q^{total}\ d_\omega^{total}]^{\mathrm{T}}$ is a vector of multi-source disturbances, where d_d^{total}, d_q^{total} are the external disturbances of the *d-q* current-loop, respectively. They can be expressed as

$$
\begin{cases}
d_d^{total} = d_d^p + d_d^{ap} \\
d_q^{total} = d_q^p + d_q^{ap}
\end{cases} \tag{3}
$$

where d_d^p and d_q^p are periodic disturbances, and

$$
\begin{cases}
d_d^p = d_{dC}^{dead} + d_{dC}^{offsets} \\
d_q^p = d_{qC}^{dead} + d_{qC}^{offsets}
\end{cases} \tag{4}
$$

where d_{dC}^{dead} and d_{qC}^{dead} are the *d-q* axis current disturbance caused by the inverter dead-time effect; $d_{dC}^{offsets}$ and $d_{qC}^{offsets}$ are the *d-q* axis current disturbances caused by the current sensor measurement.

Considering the stator current coupling components d_d^{ap}, d_q^{ap} as aperiodic disturbances, they can be expressed as follows:

$$
\begin{cases}
d_d^{ap} = n_p\omega_m i_q \\
d_q^{ap} = -\dfrac{n_p\omega_m}{L_{qo}}\left[L_{do}i_d + \psi_{ro}\right]
\end{cases} \tag{5}
$$

d_ω^{total} are the external disturbances of the speed-loop, which can be expressed as

$$d_\omega^{total} = d_\omega^p + d_\omega^{ap} \tag{6}$$

where the periodic disturbance d_ω^p is

$$d_\omega^p = d_T^{harmonics} + d_T^{cog} + d_T^{mec} \tag{7}$$

where $d_T^{harmonics}$ is the torque ripple caused by the magnetic flux harmonics, d_T^{cog} the torque ripple caused by the cogging effect, and d_T^{mec} the torque ripple caused by the motor's mechanical properties.

The aperiodic disturbance d_ω^{ap} is

$$d_\omega^{ap} = -\frac{1}{J}\left(T_L + B_m \omega_m\right) \tag{8}$$

where J is the rotational inertia actual value.

In summary, Fig. 1 shows a diagram of a PMSM drive system considering multi-source disturbances, where $\mathbf{x}^* = [i_d^* \, i_q^* \, \omega_m^*]^T$ is a vector of the reference state.

According to the frequency analysis in [1], the magnetic flux harmonics, cogging effect, and inverter dead-time effect generate $6n$-times (n is a positive integer) electrical angle subharmonic components; the zero drift of the current sensor generates 1 time electrical angle subharmonic component, while the error of the sensor gain generates two electrical angle subharmonic components.

Therefore, the electromagnetic torque ripple can be composed of 1, 2, $6n$ times electrical angle subharmonic components. It can be simplified as

$$
\begin{aligned}
T_e^{ripple} &= T_1^{ripple} - T_2^{ripple} \\
&= \sum_k T_{1k}\left[\cos\left(k\theta_e - \phi_k\right) + \sin\left(k\theta_e - \phi_k\right)\right] \\
&\quad - \sum_k T_{2k}\left[\cos\left(k\theta_e - \phi_k\right) + \sin\left(k\theta_e - \phi_k\right)\right]
\end{aligned} \tag{9}
$$

where T_1^{ripple} is the control circuit component; T_2^{ripple} is the load-side component; $k(k = 1, 2, 6n)$ is the electrical angle multiplier; T_{1k} and T_{2k} are the amplitudes of the harmonic components; and ϕ_k is the phase angle of the harmonic components.

3. ANALYSIS OF ANTI-DISTURBANCE MECHANISM OF CONVENTIONAL EID

3.1. Conventional EID Method

As shown in Fig. 1, external disturbances are imposed on the control input channel. Disturbance suppression can be achieved by designing an EID estimator for the compensation. Moreover, the compensated nominal model can suppress the impact of the system uncertainties.

According to the conventional EID framework [12], the compensated nominal model for (2) is

$$
\begin{cases}
\dot{\mathbf{x}} = \mathbf{A}_o \mathbf{x} + \mathbf{B}_o\left(\mathbf{u} + \mathbf{d}_e^{total}\right) \\
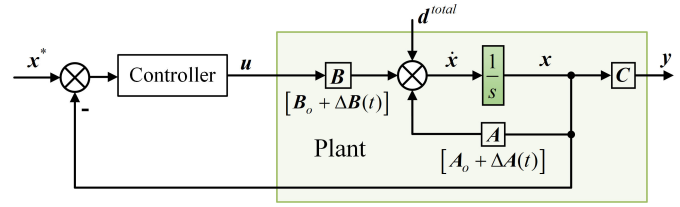\mathbf{y} = \mathbf{C}\mathbf{x}
\end{cases} \tag{10}
$$

FIGURE 1. Diagram of PMSM system considering multi-source disturbances.

where $\mathbf{d}_e^{total} = [d_{de}^{total} \, d_{qe}^{total} \, d_{\omega e}^{total}]^T$ is the EID of $\mathbf{d}^{total}$; d_{de}^{total} and d_{qe}^{total} are the EID of the current loop; $d_{\omega e}^{total}$ is the EID of the speed loop.

Design the state observer as

$$
\begin{cases}
\dot{\hat{\mathbf{x}}} = \mathbf{A}_o \hat{\mathbf{x}} + \mathbf{B}_o \mathbf{u}_f + \mathbf{L}\left(\mathbf{y} - \mathbf{C}\hat{\mathbf{x}}\right) \\
\hat{\mathbf{y}} = \mathbf{C}\hat{\mathbf{x}}
\end{cases} \tag{11}
$$

where $\mathbf{u}_f = [u_{df} \, u_{qf} \, i_{qf}]^T$ is a vector of the controller output, and $\mathbf{L} = \text{diag}(l_d, l_q, l_\omega)$ is a vector of the observer gain.

According to [12], the estimated $\mathbf{d}_e^{total}$ is

$$\hat{\mathbf{d}}_e^{total} = \mathbf{B}_o^{-1}\mathbf{L}\mathbf{C}\left[\mathbf{x} - \hat{\mathbf{x}}\right] + \mathbf{u}_f - \mathbf{u} \tag{12}$$

Filter $\mathbf{F}(s)$ is introduced to select the angular frequency components of $\hat{\mathbf{d}}_e^{total}$ to obtain the estimated disturbance. The first-order low-pass filter is given by:

$$
\begin{aligned}
\mathbf{F}(s) &= [F_d(s) \, F_q(s) \, F_\omega(s)]^T \\
&= [\frac{1}{T_d s + 1} \, \frac{1}{T_q s + 1} \, \frac{1}{T_\omega s + 1}]^T
\end{aligned} \tag{13}
$$

where T_d, T_q, and T_ω are filter time constants.

Also, the design of $\mathbf{F}(s)$ needs to satisfy

$$\mathbf{F}(j\omega) \approx 1, \quad \forall \omega \in [0, \omega_r] \tag{14}$$

where $\omega_r = [\omega_{r1} \, \omega_{r1} \, \omega_{r2}]^T$ is a vector of the disturbance highest frequency, and $\mathbf{T}_f < 1/5\omega_r$ [12].

Then, the filtered $\tilde{\mathbf{d}}_e^{total}$ of $\hat{\mathbf{d}}_e^{total}$ is obtained. Thus, the control law yields

$$\mathbf{u} = \mathbf{u}_f - \tilde{\mathbf{d}}_e^{total} \tag{15}$$

Figure 2 shows that the PMSM multi-source disturbance suppression structure based on the EID method mainly consists of an EID estimator, a state observer, and a first-order low-pass filter.
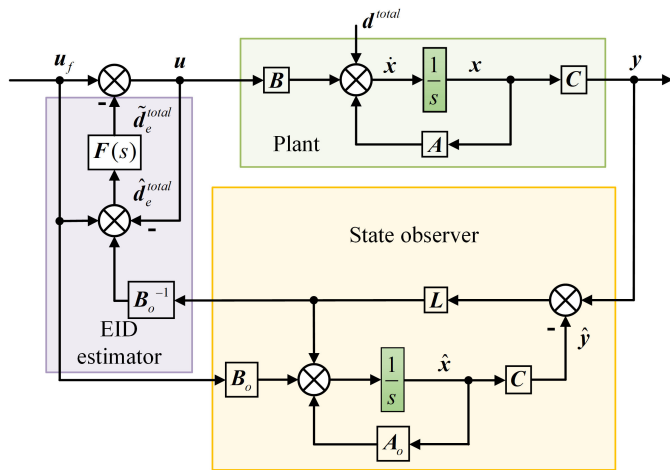
3.2. Performance Analysis of Conventional EID Method

To explore how multi-source disturbances influence the anti-disturbance performance of the EID method, the speed loop and current loop were analyzed, respectively.

3.2.1. Analysis of the Speed Loop

When the parameter perturbation occurs, the speed-loop dynamic is

$$\frac{d\omega_m}{dt} = b_\omega i_{qf} + d_\omega^{total} \tag{16}$$

FIGURE 2. Multi-source disturbances suppression mechanism based on EID method.

FIGURE 3. Frequency response of speed-loop external disturbance sensitivity function based on conventional EID.

where $b_\omega = 3n_p\psi_r/2J$ is an uncertainty coefficient; ψ_r is the PM flux uncertainty value; J is the rotational inertia actual value.

According to Fig. 2, if $i_{qf} = 0$, then the transfer function from d_ω^{total} to $\tilde{d}_{\omega e}^{total}$ is

$$G_\omega(s) = \frac{\Delta b_\omega W_\omega(s)}{1 + \Delta b_\omega W_\omega(s)} \qquad (17)$$

where $\Delta b_\omega = \frac{b_\omega}{b_{\omega o}}$, $W_\omega(s) = \frac{l_\omega}{s+l_\omega}\frac{F_\omega(s)}{1-F_\omega(s)}$.

When b_ω is perturbed, the sensitivity function of $G_\omega(s)$ is

$$S_\omega(s) = \frac{1}{1 + \Delta b_\omega W_\omega(s)} \qquad (18)$$
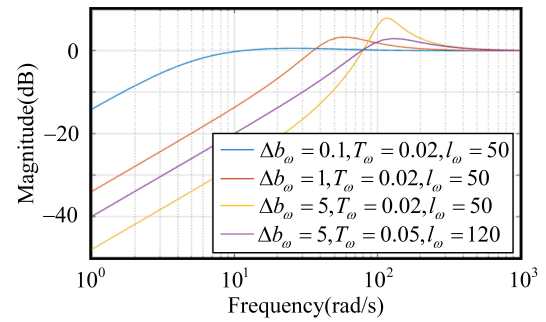
Substituting (13) into $W_\omega(s)$ yields

$$W_\omega(s) = \frac{l_\omega}{T_\omega}\frac{1}{s(s+l_\omega)} \qquad (19)$$

Substituting (19) into (18) yields

$$S_\omega(s) = \frac{s^2 + l_\omega s}{s^2 + l_\omega s + \frac{\Delta b_\omega l_\omega}{T_\omega}} \qquad (20)$$

Figure 3 shows the frequency response of the speed loop sensitivity function for different parameters. As illustrated in Fig. 3, when $\Delta b_\omega \ll 1$, the frequency response of $S_\omega(s)$ is generally below 0 dB, demonstrating effective disturbance suppression. The low-frequency disturbance components are effectively suppressed, and the impact of high-frequency disturbances is not amplified. However, when $\Delta b_\omega \geq 1$, the sensitivity function exhibits the "waterbed effect", and unstable risks emerge in the relatively high-frequency band.

According to the Bode integral theorem [14], it can be seen that the relative order of $S_\omega(s)$ is 2, and the amplitude frequency characteristic rises at a slope of $+40$ dB/10n. Compared to designs with orders of less than 2, high frequency sensitivity must be sacrificed to obtain better low-frequency performance. When parameter perturbation occurs, the possibility of unstable risk in the speed loop increases with high-frequency components above $6n$ order in multi-source disturbances.

3.2.2. Analysis of the Current Loop

Because the d-q-axis current-loop analysis process is consistent, only the q-axis was analyzed. When parameter perturbation occurs, the dynamic is

$$\frac{di_q}{dt} = a_q i_q + b_q u_{qf} + d_q^{total} \qquad (21)$$

where $a_q = -R_s/L_q$, and $b_q = 1/L_q$ are uncertain coefficients. R_s is an uncertain resistance. L_q is an uncertain q-axis inductance.

Let $u_{qf} = 0$, the transfer function from d_q^{total} to $\tilde{d}_{qe}^{total}$ is

$$G_q(s) = \frac{\Delta b_q W_q(s)}{1 + \Delta b_q W_q(s)} \qquad (22)$$

where $\Delta b_q = b_q/b_{qo}$, $W_q(s) = \frac{1}{s-a_q}\frac{l_q(s-a_{qo})}{s+(l_q-a_{qo})}\frac{F_q(s)}{1-F_q(s)}$.

When R_s is perturbed, the sensitivity function of $G_q(s)$ is

$$S_{q1}(s) = \frac{a_q(s-a_q)[1+\Delta b_q W_q(s)]}{\{[s+(s-a_q)\Delta b_q W_q(s)] - a_q\}^2} \qquad (23)$$

Substituting (13) into $W_q(s)$ yields

$$W_q(s) = \frac{l_q}{T_q}\frac{s-a_{qo}}{s(s-a_q)[s+(l_q-a_{qo})]} \qquad (24)$$

Owing to the complexity of substituting $W_q(s)$ into $S_{q1}(s)$ for calculation, a qualitative analysis of the system performance under only R_s perturbations can be conducted. Substituting (24) into (22) yields

$$G_q(s) = \frac{\Delta b_q l_q(s-a_{qo})}{T_q s(s-a_q)[s+(l_q-a_{qo})] + \Delta b_q l_q(s-a_{qo})} \qquad (25)$$

Equation (25) demonstrates that the relative order of the current loop sensitivity function is two when only R_s is perturbed.
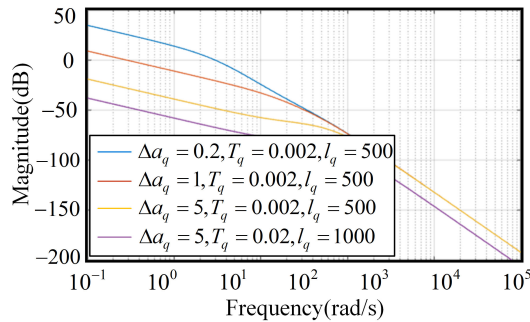
When both R_s and L_q are perturbed, the sensitivity function of $W_q(s)$ is

$$S_{q2}(s) = \frac{l_q(s-a_{qo})}{(s-a_q)^2[s+(l_q-a_{qo})]}\frac{F_q(s)}{1-F_q(s)} \qquad (26)$$

Substituting (13) into (26) yields

$$S_{q2}(s) = \frac{l_q}{T_q} \frac{(s - a_{qo})}{s (s - a_q)^2 [s + (l_q - a_{qo})]} \qquad (27)$$

Let $\Delta a_q = a_q/a_{qo}$. As shown in Fig. 4, when $\Delta a_q \leq 1$, $S_{q2}(s)$ exhibited an amplitude significantly above 0 dB in the low-frequency band with a relatively large peak, indicating a narrow system stability margin and a pronounced amplification effect on low-frequency disturbances. It reveals that when parameter perturbation occurs, low-frequency components such as 1- and 2-times order in multi-source disturbances will increase the possibility of unstable risk in the current loop.

FIGURE 4. Frequency response of current-loop external disturbance sensitivity function based on conventional EID.

Equation (27) indicates that when both R_s and L_q are perturbed, the relative order of the current loop sensitivity function is three, which worsens its impact.

4. IMPROVED EID METHOD

4.1. Design of Enhanced Estimator

Section 3 reveals that, considering parameter perturbation, the speed-loop sensitivity function has a relative order of two, while the current-loop sensitivity function has a relative order of three. Consequently, excessive emphasis on suppressing disturbances in a specific frequency band may compromise the stability. A viable strategy to overcome this limitation is to lower the relative order of the sensitivity function, which strikes a balance between high and low frequencies.

The enhanced speed-loop estimator is designed as

$$F_\omega(s) = \frac{T_\omega s + 1}{\mu T_\omega s + 1} \qquad (28)$$

The enhanced current-loop estimator is designed as

$$F_q(s) = \frac{s}{s + (\mu - 1)} \qquad (29)$$

where $\mu > 1$ is a balance coefficient between the high-frequency anti-disturbance capability and system response speed. For (28), increasing μ can reduce the bandwidth of the filter and decrease high-frequency sensitivity, but it will also increase the time delay of high-frequency disturbance

estimation. For (29), μ directly affects the distribution of zeros and poles of the filter, thereby altering the suppression capability of the current-loop for low-frequency disturbances.

Substituting (28) into $W_\omega(s)$ yields

$$W_\omega(s) = \frac{l_\omega}{(\mu - 1) T_\omega} \frac{T_\omega s + 1}{s (s + l_\omega)} \qquad (30)$$

Substituting (29) into (26) yields

$$S_{q2}(s) = \frac{l_q}{(\mu - 1)} \frac{s (s - a_{qo})}{(s - a_q)^2 [s + (l_q - a_{qo})]} \qquad (31)$$

Equations (30) and (31) demonstrate that the sensitivity functions of the speed and current loops are both reduced to one order of magnitude. This effectively avoids the "waterbed effect" and enhances system robustness.

Figure 5 demonstrates that when parameter perturbation occurs, the gain margin of the speed loop decreases below 0 dB in the high-frequency band, whereas the gain margin of the current loop decreases below 0 dB in the low-frequency band. The results reveal that the enhanced estimators effectively increase the capacity for disturbance suppression across different frequency bands, thereby extending the applicability of the EID method.

Remark 1: *The the d-axis current-loop estimator has the same design as the q-axis current-loop estimator.*

4.2. System Stability Analysis

The preceding analysis focused solely on optimizing the influence of external disturbances. However, the impact of uncertainties (i.e., parameter perturbation) requires further analysis. Let $\mathbf{d}^{total} = 0$ to analyze the stability of the nominal model. Considering the PI controller, simplifying the block diagram in Fig. 2 yields Fig. 6.

Substituting (29) into (22) yields

$$W_q(s) = \frac{l_q}{\mu - 1} \frac{s (s - a_{qo})}{(s - a_q) [s + (l_q - a_{qo})]} \qquad (32)$$

Based on (30) and (32), the open-loop transfer functions of the speed loop and the current loop are obtained, respectively.

$$G_\omega^{op}(s) = \frac{\Delta b_\omega \left(P_\omega + \frac{I_\omega}{s}\right)}{s} \frac{1 + W_\omega(s)}{1 + \Delta b_\omega W_\omega(s)}$$

$$= \frac{\Delta b_\omega \left(P_\omega s + I_\omega\right) \left[s^2 + \left(l_\omega + \frac{l_\omega}{\mu - 1}\right) s + \frac{l_\omega}{(\mu - 1) T_\omega}\right]}{s^2 \left[s^2 + \left(l_\omega + \frac{\Delta b_\omega l_\omega}{\mu - 1}\right) s + \frac{\Delta b_\omega l_\omega}{(\mu - 1) T_\omega}\right]} \qquad (33)$$

$$G_q^{op}(s) = \frac{\Delta b_q \left(P_c + \frac{I_c}{s}\right)}{s - a_q} \frac{1 + W_q(s)}{1 + \Delta b_q W_q(s)}$$

$$= \frac{\Delta b_q \left(P_c s + I_c\right)}{s (s - a_q)}$$
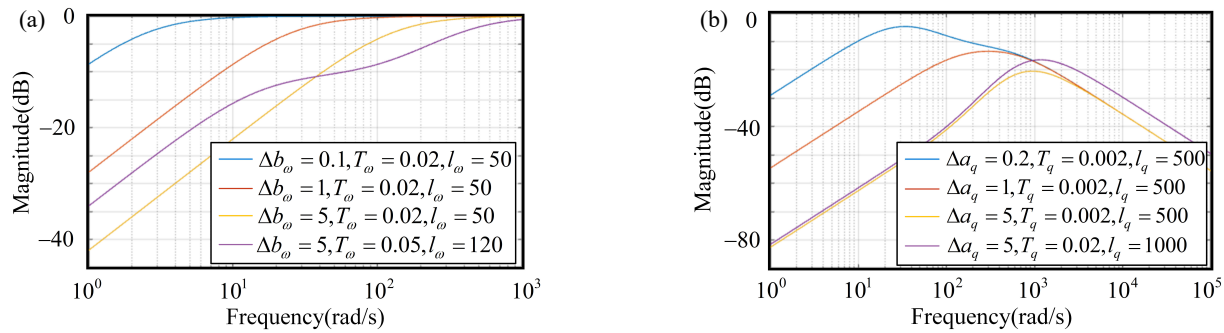
FIGURE 5. Frequency response of external disturbance sensitivity function based on IEID method. (a) Speed-loop. (b) Current-loop.
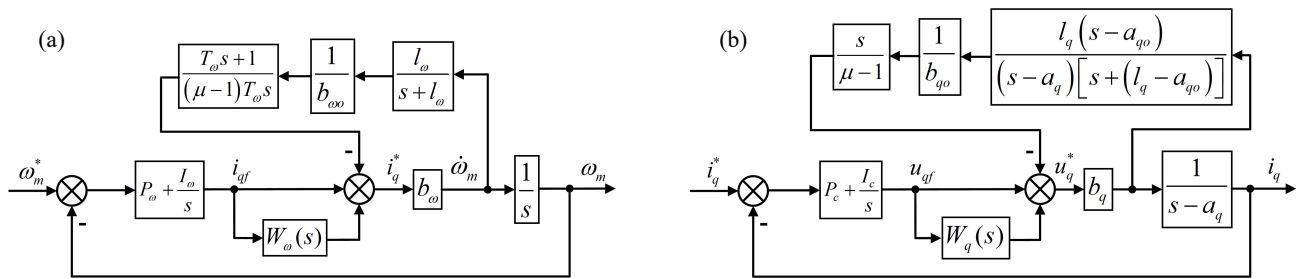
FIGURE 6. Diagram of open-loop transfer function without external disturbances. (a) Speed-loop. (b) Current-loop.

$$\frac{\left\{s^2 + \left[\frac{(\mu-1)(l_q-a_q-a_{qo})-l_q a_{qo}}{(\mu-1)+l_q}\right] s + \frac{(\mu-1)a_q(a_{qo}-l_q)}{(\mu-1)+l_q}\right\}}{\left\{s^2 + \left[\frac{(\mu-1)(l_q-a_q-a_{qo})-\Delta b_q l_q a_{qo}}{(\mu-1)+\Delta b_q l_q}\right] s + \frac{(\mu-1)a_q(a_{qo}-l_q)}{(\mu-1)+\Delta b_q l_q}\right\}} \qquad (34)$$

Equation (33) shows that when the relative order of $G_\omega^{op}(s)$ is one, there is only one root locus trajectory with an asymptote that tends to infinity. This asymptote intersects the real axis at σ_α, and the intersection angle is $90°$. The σ_α is

$$\sigma_\alpha = -\frac{\Delta b_\omega l_\omega}{\mu - 1} + \frac{l_\omega}{\mu - 1} + \frac{I_\omega}{P_\omega} \qquad (35)$$

According to (35), the condition for the root locus of $G_\omega^{op}(s)$ to remain in the left half of the complex plane is

$$-\frac{\Delta b_\omega l_\omega}{\mu - 1} + \frac{I_\omega}{P_\omega} + \frac{l_\omega}{\mu - 1} < 0 \qquad (36)$$

where $\Delta b_\omega > 1$ makes Equation (36) hold.

As shown in Equation (34), it can be seen that the relative order of $G_q^{op}(s)$ is 1. Assuming that l_q is very large, (33) can be simplified as

$$G_q^{op}(s) = \frac{\Delta b_q (P_c s + I_c)\left\{s^2 + (\mu-1-a_{qo})\,s - (\mu-1)\,a_q\right\}}{(s - a_q)\left\{s^2 + \frac{(\mu-1-\Delta b_q a_{qo})}{\Delta b_q} s - \frac{(\mu-1)a_q}{\Delta b_q}\right\}} \qquad (37)$$

Then, $G_q^{op}(s)$ has only one root locus branch that tends towards infinity along an asymptote, which intersects the real axis

at σ_β, and the intersection angle is $90°$. Thus, we obtain

$$\begin{cases} \sigma_\beta = a_q + p_2 + \dfrac{I_c}{P_c} - z_2 \\[2mm] p_2 = \dfrac{-(\mu-1-\Delta b_q a_{qo}) + \sqrt{(\mu-1-\Delta b_q a_{qo})^2 - 4(\mu-1)\,a_q}}{2\Delta b_q} \\[2mm] z_2 = \dfrac{-(\mu-1-a_{qo}) + \sqrt{(\mu-1-a_{qo})^2 - 4(\mu-1)\,a_q}}{2} \end{cases} \qquad (38)$$

According to (38), the condition for the root locus of $G_q^{op}(s)$ to remain in the left half of the complex plane is

$$\frac{I_c}{P_c} < z_2 - p_2 - a_q \qquad (39)$$

Equation (39) shows that setting a large gain for the EID of the current loop and adjusting the PI controller can mitigate the instability risk.

Based on (36), (38), and (39), the value of μ must satisfy the derived stability conditions. Generally, it is recommended to set $2 \le \mu \le 5$, which is determined by system bandwidth and the main frequency component of the disturbance.

Therefore, the nominal model considering $\mathbf{d}^{total} = 0$ is Bounded-Input Bounded-Output (BIBO) stable. Since the IEID structure, consisting of observers and IEID estimators, is also BIBO stable, according to the small-gain theorem [15], the system considering $\mathbf{d}^{total} \ne 0$ is stable.
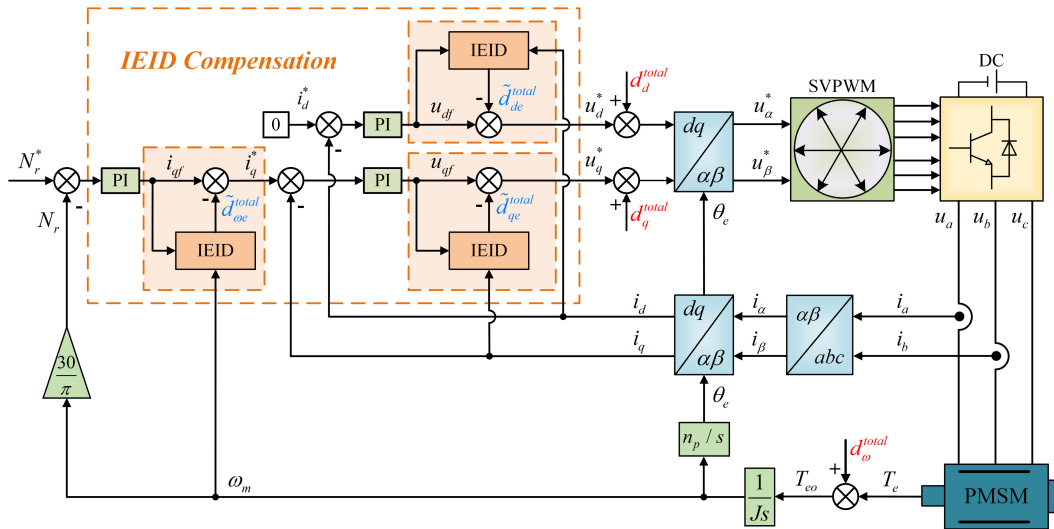
FIGURE 7. Diagram of multi-source disturbances suppression for PMSM based on IEID.

5. SIMULATION VERIFICATION

As shown in Fig. 7, we applied the proposed IEID method to a surface-mounted PMSM (SPMSM) drive system. The reference speed was set to 2000 rpm with a slow start. The start time is 0.01 s, and the initial load is set to $2\,\mathrm{N\cdot m}$.

The external disturbances are set to

$$
\begin{cases}
d_d^{total} = 7\sin 36\pi t + 3\sin\left(18\pi t + \dfrac{\pi}{6}\right) \\
\qquad + 2\cos\left(6\pi t + \dfrac{\pi}{3}\right) + \sin\left(\pi t + \dfrac{\pi}{6}\right) \\
d_q^{total} = 7\cos 36\pi t + 3\cos\left(18\pi t + \dfrac{\pi}{6}\right) \\
\qquad + 2\cos\left(6\pi t + \dfrac{\pi}{3}\right) + \cos\left(\pi t + \dfrac{\pi}{6}\right) \\
d_\omega^{total} = -\left(0.03\cos 12\pi t + 0.05\sin 36\pi t\right. \\
\qquad \left. -T_L - B_m\omega_m\right)
\end{cases}
\tag{40}
$$

The principles of parameter adjustment are as follows:

(i) The gain of PI controllers must satisfy the constraints of (36) and (39).

(ii) Based on (36) and (39), on the premise of satisfying stability, select appropriate T_ω and μ to balance the high-frequency anti-disturbance capability and system response speed.

The SPMSM parameters are listed in Table 1. The vector control with $i_d = 0$ was performed.

Simulation comparisons were conducted using these four methods as shown in Table 2. The ISMO-EID method mentioned in Table 2 is an improved EID method proposed by Huang et al. [16]. It replaces the linear observer in the conventional EID framework with an improved sliding mode observer. This enhancement improves disturbance suppression

TABLE 1. Nominal parameters of SPMSM.

Parameters	Unit	Values
DC voltage (U_N)	V	1500
Stator resistance (R_s)	Ω	1.4
Number of pole pairs (n_p)	pairs	3
Stator inductance (L_s)	mH	8.5
Rotor PM flux (ψ_r)	Wb	0.175
Rotational Inertia (J)	kg $\cdot$ m^2	0.01
Viscous friction coefficient (B_m)	N $\cdot$ m $\cdot$ s/rad	0.0008

performance by increasing the estimation accuracy of EID. The block diagram of ISMO-EID method is shown in Fig. 8. In these comparisons, all the PI controllers were set to the same value. The gain of the speed loop PI controller was set to $P_\omega = 0.5$, $I_\omega = 12.5$ and the current loop set to $P_c = 9.35$, $I_c = 1311.2$.
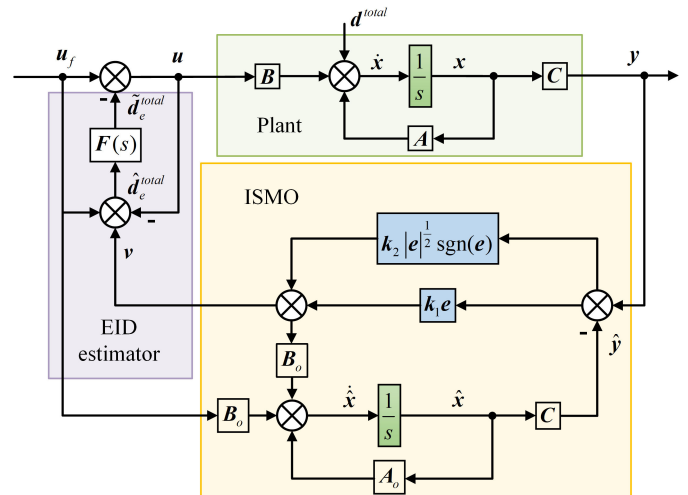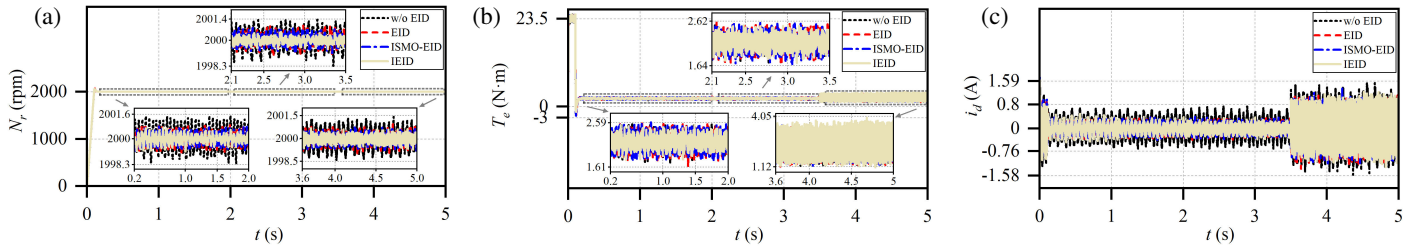

FIGURE 8. Block diagram of ISMO-EID method.

FIGURE 9. Comparison of steady-state performance. (a) Speed. (b) Torque. (c) d-axis current.
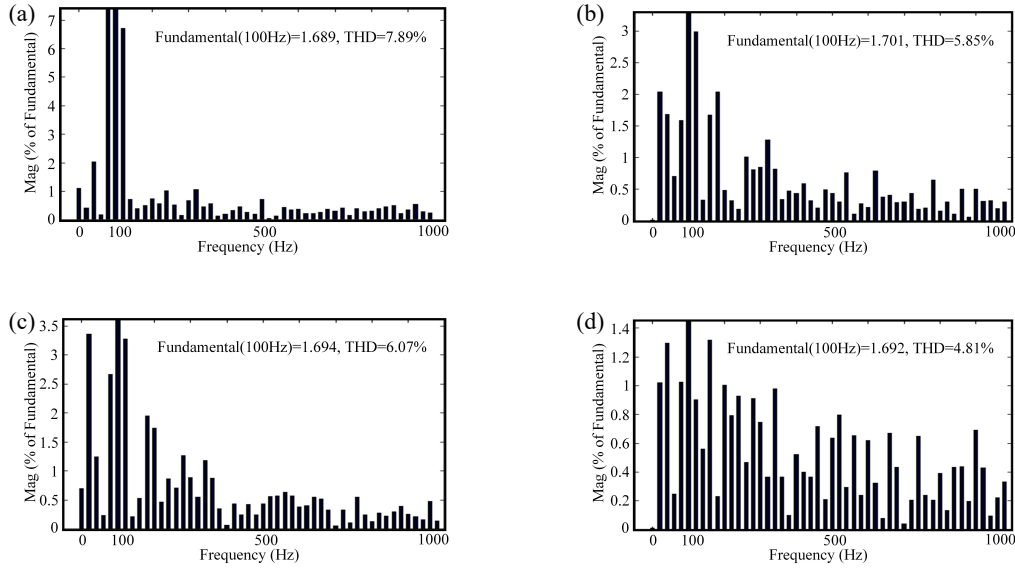

FIGURE 10. THD analysis of A-phase current under parameter perturbation. (a) Without EID. (b) EID. (c) ISMO-EID. (d) IEID.

TABLE 2. Control method.

Scheme	Control method
Scheme 1	without EID
Scheme 2	EID
Scheme 3	ISMO-EID
Scheme 4	IEID

The parameter settings for the EID and IEID segments were set to: $l_d = l_q = 500$; $l_\omega = 150$; $T_d = T_q = 0.002$; $T_\omega = 0.02$; $\mu = 3$. The ISMO-EID method uses the same one-order low-pass filter as EID method, since the gain $\mathbf{k}_1$ and linear gain $\mathbf{L}$ play the same role; set $\mathbf{k}_1 = \mathbf{L}\mathbf{B}_o^{-1}$; unfolding $\mathbf{k}_1$ gets $k_{d1} = k_{q1} = 4.25$, $k_{\omega 1} = 1.52$; unfolding $\mathbf{k}_2$ gets $k_{d2} = k_{q2} = 0.1$, $k_{\omega 2} = 10$.

5.1. Steady-State Operation Analysis

To verify the applicability of the IEID method, the parameters perturbation for the speed-loop was set at 2 s: b_ω increases to $1.36b_{\omega o}$, then $\Delta b_\omega = 1.36$. The parameters perturbation for the current-loop was set at 3.5 s: a_d and a_q decrease to $0.3a_{do}$ and $0.3a_{qo}$, then $\Delta a_q = \Delta a_d = 0.3$.

Figure 9(a) illustrates the speed fluctuations of the four methods. During 0.2 to 2 seconds, the motor operates under nominal parameters. The speed fluctuation peak-to-peak values (PPVs)

of the method without EID, EID, ISMO-EID, and IEID are 3.3, 1.88, 1.62, and 1.22 RPM, respectively. During 2.1 to 3.5 seconds, the speed fluctuation PPVs of the method without EID, EID, ISMO-EID, and IEID are 3.1, 2.01, 1.66, and 1.13 RPM, respectively. During 3.6 to 5 seconds, the speed fluctuation PPVs of the method without EID, EID, ISMO-EID, and IEID are 2.89, 2.02, 1.59, and 1.41 RPM, respectively. These results demonstrate that the proposed IEID method achieves an optimal speed stability and disturbance suppression.

Figure 9(b) shows the fluctuations in the torques of the four methods. During 0.2 to 2 seconds, the IEID method suppressed approximately 22% of the torque fluctuations, while the EID and ISMO-EID methods had almost no effect. However, from 3.6 to 5 s, when parameter perturbations occurred in the current loop, all the methods lost their anti-disturbance capability. In addition, at 0.1 s, the torque negative chatter of the IEID method is minimal, which means that its robustness is the best during the speed-up process.

Figure 9(c) shows the necessity of the EID compensation for the d-axis current-loop. Compared to the case without EID, the EID method and ISMO-EID significantly suppressed d-axis current fluctuations, and the IEID method further improved the suppression effect. According to Equation (5), this is equivalent to suppressing the aperiodic disturbance of the q-axis current loop. Therefore, it is beneficial to suppress the torque fluctuations.
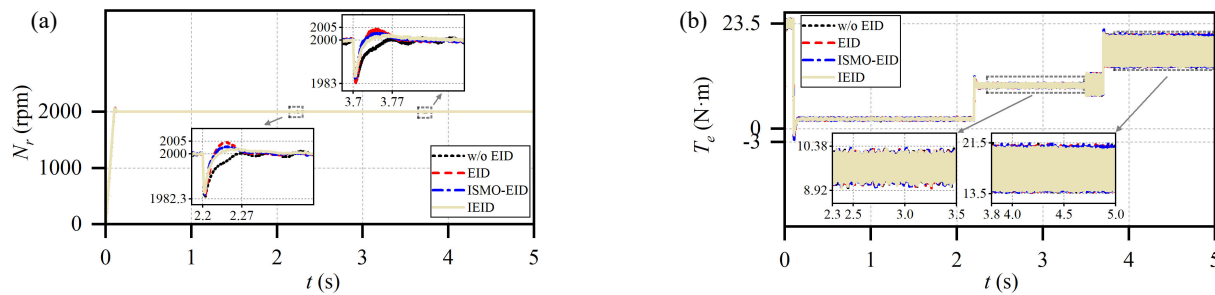
FIGURE 11. Comparison of transient-state performance. (a) Speed. (b) Torque.

To further verify the effectiveness of the presented IEID method, an FFT analysis was performed on the A-phase stator current from 3.6 to 5 s, which corresponds to the parameter perturbation. As shown in Fig. 10, when the parameter perturbation occurred, the THD index was 7.89% for the method without EID, while the THD indices of the EID method and ISMO-EID were 5.85% and 6.07%. Moreover, the IEID method reduces the THD index to 4.81%. These results indicate that the proposed IEID method achieves the best disturbance suppression effect.

5.2. Transient Operation Analysis

During the transient operation, the original operating conditions were maintained. A sudden increase in load torque of $7.5\,\mathrm{N\cdot m}$ was set at 2.2 s and 3.7 s, respectively. The simulation results are shown in Fig. 11.

As shown in Fig. 11(a), the speed fluctuation PPV using the EID method and ISMO-EID reached 22.7 and 20.2 RPM after loading. However, the control of the IEID method optimized the speed fluctuation PPV to 17.8 RPM, reducing the amplitude of negative fluctuations and revealing better robustness. It is worth noting that the introduction of the EID method will slightly reduce the dynamic response speed.

When comparing Fig. 9(b) and Fig. 11(b), it can be seen that no matter after the initial loading at 2.2 s or 3.7 s, the EID method can still only suppress approximately 20% of the torque fluctuation. However, the EID and ISMO-EID methods had almost no effect.

6. CONCLUSION

An active disturbance suppression strategy, termed "improved equivalent-input-disturbance (IEID) method based on enhanced estimators" is presented to address the control performance degradation in the PMSM drive system caused by multi-source disturbances in different frequency bands. A PMSM model that considers multi-source disturbances was established. The estimated EID configuration was integrated into both the current and speed loops to counteract disturbances by compensation. An analysis of the anti-disturbance mechanism reveals that the system controlled by the conventional EID method is prone to instability under parameter perturbation. Specifically, this leads to vulnerability of the speed-loop to high-frequency disturbances and the current loop to low-frequency disturbances. Subsequently, several enhanced

estimators were designed to reduce the relative order of the sensitivity function to 1, thereby eliminating the limitations of the EID method and expanding the bandwidth for disturbance suppression. The simulation confirmed the effectiveness of the IEID method and showed superior performance in both steady and transient states.

It is noteworthy that the EID method is an active disturbance rejection method. Our future research will concentrate on integrating the EID with robust control and SMC.

REFERENCES

[1] Yang, J., W.-H. Chen, S. Li, L. Guo, and Y. Yan, "Disturbance/uncertainty estimation and attenuation techniques in PMSM drives — A survey," *IEEE Transactions on Industrial Electronics*, Vol. 64, No. 4, 3273–3285, 2017.

[2] Wei, Q., L. Dong, W. Li, M. Andriollo, and D. Zeng, "Comparative analysis of electromagnetic vibration and torque ripple of multi-unit PMSMs under normal and fault operation," *IEEE Transactions on Magnetics*, Vol. 61, No. 9, 1–6, 2025.

[3] Cheng, M., Z. Xu, Y. Jiang, and C. Zhao, "Investigation of cogging torque generation mechanisms in flux-switching permanent magnet machines based on general air-gap field modulation theory," *Chinese Journal of Electrical Engineering*, Vol. 11, No. 2, 207–215, 2025.

[4] Hu, M., W. Hua, Z. Wu, N. Dai, H. Xiao, and W. Wang, "Compensation of current measurement offset error for permanent magnet synchronous machines," *IEEE Transactions on Power Electronics*, Vol. 35, No. 10, 11 119–11 128, 2020.

[5] Kim, S.-Y., W. Lee, M.-S. Rho, and S.-Y. Park, "Effective deadtime compensation using a simple vectorial disturbance estimator in PMSM drives," *IEEE Transactions on Industrial Electronics*, Vol. 57, No. 5, 1609–1614, 2010.

[6] Dorrell, D. G., J. K. H. Shek, M. A. Mueller, and M.-F. Hsieh, "Damper windings in induction machines for reduction of unbalanced magnetic pull and bearing wear," *IEEE Transactions on Industry Applications*, Vol. 49, No. 5, 2206–2216, 2013.

[7] Zhang, J., W. Ren, and X.-M. Sun, "Current-constrained adaptive robust control for uncertain PMSM drive systems: Theory and experimentation," *IEEE Transactions on Transportation Electrification*, Vol. 9, No. 3, 4158–4169, 2023.

[8] Zhang, Z., X. Yang, W. Wang, K. Chen, N. C. Cheung, and J. Pan, "Enhanced sliding mode control for PMSM speed drive systems using a novel adaptive sliding mode reaching law based on exponential function," *IEEE Transactions on Industrial Electronics*, Vol. 71, No. 10, 11 978–11 988, 2024.

[9] Wu, Z.-H., H.-C. Zhou, F. Deng, and B.-Z. Guo, "Disturbance observer-based boundary control for an antistable stochastic heat equation with unknown disturbance," *IEEE Transactions on Automatic Control*, Vol. 68, No. 6, 3604–3611, 2023.

[10] Cao, H., Y. Deng, Y. Zuo, X. Liu, J. Wang, and C. H. T. Lee, "A variable structure ADRC for enhanced disturbance rejection and improved noise suppression of PMSM speed system," *IEEE Transactions on Industrial Electronics*, Vol. 72, No. 5, 4481–4495, 2025.

[11] She, J.-H., X. Xin, and Y. Pan, "Equivalent-input-disturbance approach — Analysis and application to disturbance rejection in dual-stage feed drive control system," *IEEE/ASME Transactions on Mechatronics*, Vol. 16, No. 2, 330–340, 2011.

[12] She, J.-H., M. Fang, Y. Ohyama, H. Hashimoto, and M. Wu, "Improving disturbance-rejection performance based on an equivalent-input-disturbance approach," *IEEE Transactions on Industrial Electronics*, Vol. 55, No. 1, 380–389, 2008.

[13] Du, Y., W. Cao, J. She, M. Wu, M. Fang, and S. Kawata, "Disturbance rejection and robustness of improved equivalent-input-disturbance-based system," *IEEE Transactions on Cybernetics*, Vol. 52, No. 8, 8537–8546, 2022.

[14] Stein, G., "Respect the unstable," *IEEE Control Systems Magazine*, Vol. 23, No. 4, 12–25, 2003.

[15] Zhou, K. and J. C. Doyle, *Essentials of Robust Control*, Upper Saddle River, NJ, Prentice Hall, 1998.

[16] Huang, G., J. Li, E. F. Fukushima, C. Zhang, J. He, and K. Zhao, "An improved equivalent-input-disturbance approach for PMSM drive with demagnetization fault," *ISA Transactions*, Vol. 105, 120–128, 2020.